 CMES, vol.72, no.4, pp.273-297, 2011

A Nonlinear Dynamic Model for Periodic Motion of Slender Threadline Structures

Jinling Long[1,2], Bingang Xu[1,3] and Xiaoming Tao[1]

Abstract: Moving slender threadline structures are widely used in various engineering fields. The dynamics of these systems is sometimes time dependent but in most cases follows a periodic pattern, and slender yarn motion in textile engineering is a typical problem of this category. In the present paper, we propose a nonlinear approach to model the dynamic behavior of slender threadline structures with a real example in the analysis of slender yarn motion in spinning. Moving boundary conditions of yarn are derived and a consequence of the perturbation analysis for the dimensionless governing equations provides the zero order approximate equation of motion to remove the time dependence. Consequently, the time dependent problem can be solved by approximate solutions of steady-state governing equations subject to the derived moving boundary conditions. The simulation results are more accurate than the results by earlier work and show good agreement with measurement data. The proposed modeling and perturbation approximation procedure is thus an accurate and practical way to deal with periodical motion of a category of slender threadline structures.

Keywords: nonlinear analysis, dynamic model, perturbation analysis, threadline structure

1 Introduction

A diverse range of disciplinaries in life science and engineering involves large motions of slender thread like bodies or structures such as DNA, hair, cable, rope, fiber and yarn [Jurak and Tambca, 1999; O'Reilly, 1996; Coleman, Olson and Swigon, 2003; Kmoch, Bonanni and Magnenat-Thalmann, 2009; Guo and Xu, 2010; Tang and Advani, 2005; Guo and Xu, 2009; Fraser, Ghosh and Batra, 1992]. Thus, the steady or unsteady dynamic analysis on the motion of a moving threadline under

[1] Institute of Textiles and Clothing, the Hong Kong Polytechnic University, Kowloon, Hong Kong
[2] Department of Mathematics, Southeast University, Nanjing, China
[3] Corresponding author. Email address: tcxubg@inet.polyu.edu.hk.

various boundary conditions is of particular interest and importance to researchers in physics, biology and engineering [Fraser, Ghosh and Batra, 1992; Kinkaid and O'Reilly, 2001; Tang, Xu and Tao, 2010; Tang, Xu, Tao and Feng, 2011; Clark, Fraser and Stump, 2001; Luo, 2000; Yang, Wu and Wang, 2009; Yang, Fang, Chen and Zhen, 2009]. In most unsteady problems, though the elements and the system parameters are time-dependent, some of them are not arbitrary and indeed follow a periodic pattern. For the modeling of slender threadline structures, nonlinear rod theories are commonly used to understand the mechanics of thin long rods with length scales much larger than the lateral dimensions of the structure. Mathematically, a rod is modeled as a curve in 3D space with effective mechanical properties such as bending and torsional stiffness. In the past, much effort has been made to examine static equilibrium problems and instability of slender threadline structures [Lu and Perkins, 1994; Coyne, 1990; Lu and Perkins 1995; Tobias, Swigon and Coleman, 2000; Heijden, Neukirch, Goss and Thompson, 2003]. However, there are few investigations on nonlinear dynamic responses and computations for them due to the mathematical complexities incurred in modeling. For this category of objects with periodic dynamics, an approximate modeling approach is, therefore, more desirable and practical for usage because of the adequate accuracy and reduced complexities incurred in the analysis. In this paper, we attempt to model the dynamic behavior of a typical slender body of yarn when it slides over a navel surface in spinning. A new deviation of moving boundary and periodic conditions are developed, and then the perturbation analysis is used to formulate the zero order approximation of the equations of motion and the periodic dynamics can be approximated by solving a stationary problem subject to the moving boundary conditions. Thus, we can remove the time dependence from the governing equations and consequently the time dependence of the approximation to the solution is solely controlled by the proposed moving boundary conditions. This procedure would provide a simple and practical method to model large periodic motions of thin thread like bodies.

As a real application of this proposed modeling method, dynamics of slender yarns produced in rotor spinning will be theoretically and numerically analyzed. Yarn made from natural fibers, carbon nanotubes or other types of fibrous materials is all formed by twisting an assembly of short or long fibers. During this process, the dynamics of yarn running on the navel surface is of fundamental importance to the stability and continuity of yarn formation and its variation may result in possible decrease in yarn qualities [Grosberg and Monsour, 1975; Narayana, 2005]. Although several authors have attempted to investigate this mechanism [Guo, Tao and Lo, 2000; Xu and Tao, 2003; Wang and Huang, 2000; Yu, Cai, Wu and Chen, 2007], their analysis are all based on the steady state assumption, namely all parameters

being time-independent. Under this framework, tension distribution is assumed to be independent of time and solely vary along yarn length during spinning. This kind of treatment may be appropriate when the yarn leaves the navel directly along the doffing tube (i.e., exactly along the global $-Z'$ ($-Z$) axis of the rotating frame in Figure 3). However, this is not true in practice. As shown in Figure 5, the yarn slides on the stationary navel, then leaves the navel at the leaving point Q_1, and finally moves out through the doffing tube at a fixed point A. Because of the fixed point A, the leaving point of the yarn will move forward and backward along a special trajectory as shown in Figure 4 and the boundary conditions of the yarn at the leaving point Q_1 is thus time varying. As the leaving point of the yarn moves forward and backward along its trajectory, the yarn motion on the navel is periodic. Thus, the purpose of the present study is to give a dynamic analysis of the yarn between the entrance point Q_0 and the leaving point Q_1. The boundary conditions at the leaving point are derived by its motion and the continuity conditions of velocity. In this analysis, we approximate the periodic yarn dynamics by solving a stationary problem subject to the modified boundary conditions at the leaving point. Perturbation analysis is then used to simplify the time varying motion problem to a sequence of stationary motion problems with boundary conditions that are periodic functions of time.

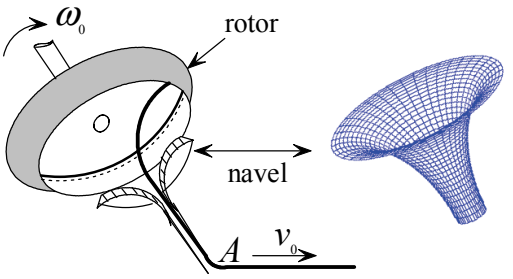

Figure 1: Schematic view of yarn motion in rotor spinning.

This paper is organized as follows. We will develop the dynamic model of yarn motion on the navel with derivation of the new boundary conditions at the leaving point in Section 2. In Section 3, the motion equations will be expressed in terms of dimensionless variables. The perturbation analysis is then used to approximate the equation of yarn motion in this section. In Section 4, numerical results are provided and discussed in detail. Finally, the conclusion is drawn in Section 5.

2 Nonlinear Dynamic Modeling

To analyze the movement of yarn, we first introduce the yarn formation process of rotor spinning. The individual fibers are blown into the rotor continually and rotate with the rotor at a high angular speed. The fibers are then located at the circumferences notch of rotor due to the centrifugal force. The yarn-like fibers are then peeled off from the rotor notch and come into the free space between the rotor and the navel. Each revolution of the yarn at this point inserts a turn of twist. Afterwards, the yarn passes through the navel surface and the doffing tube successively. The yarn from the peeling off point of rotor notch to the leaving point on the navel has constant delivery speed and rotates along with the rotor simultaneously. The schematic view of the yarn in rotor spinning is demonstrated in Figure 1. In the above mentioned process, the dynamic behaviors of the yarn on the navel are most concerned. Suppose point P is an infinitesimal element of the yarn on the navel, which at time t has a distance s from the entrance point Q_0 (s= 0). For the convenience of analysis, we choose a cylindrical reference frame with base vectors $\mathbf{e}_r$, $\mathbf{e}_\phi$, $\mathbf{e}_z$, which rotates about the Z axis of the inertial frame O– XYZ with a constant angular speed $\omega\mathbf{e}_z$, as shown in Figure 2.

The origin O coincides with the center of the smaller navel aperture, and the Z axis of the frame is in line with the central axis of the navel with its positive direction towards the rotor. Let r, ϕ, z be the cylindrical coordinates corresponding to the rotating coordinate system and $R(s,t) = r\mathbf{e}_r + z\mathbf{e}_z$ be the position vector of Prelative to the origin O. The yarn is confined to the navel surface, thus r and z satisfy the navel geometry equation. As shown in Figure 3, the profile of navel in rotor spinning is usually formed by a rotational surface, and its parametric equation is R= $g(\theta)$ $\mathbf{e}_r$+ $f(\theta)$ $\mathbf{e}_z$. The functions $g(\theta)$ and $f(\theta)$ are given by

$$r = g(\theta) = r_m + r_0(1-\cos\theta), \tag{1}$$

and

$$f(\theta) = r_0 \sin\theta, \tag{2}$$

where r_m and r_0 are constant parameters of navel profile,r_m is the radius of the smaller navel aperture, r_0 is the hight of the navel, and the generate functions $g(\theta)$ and $f(\theta)$ are shown in Figure 3.

Thus, the coordinates of yarn element P in the inertial frame are

$$([r_m + r_0(1-\cos\theta)]\cos\phi,\ [r_m + r_0(1-\cos\theta)]\sin\phi, r_0\sin\theta).$$

It can be observed that the position vector of the yarn can be determined by the parameters θ and ϕ. Without loss of generality, ω is assumed to be constant, provided ω is chosen to be an appropriate mean angular speed of the leaving point of

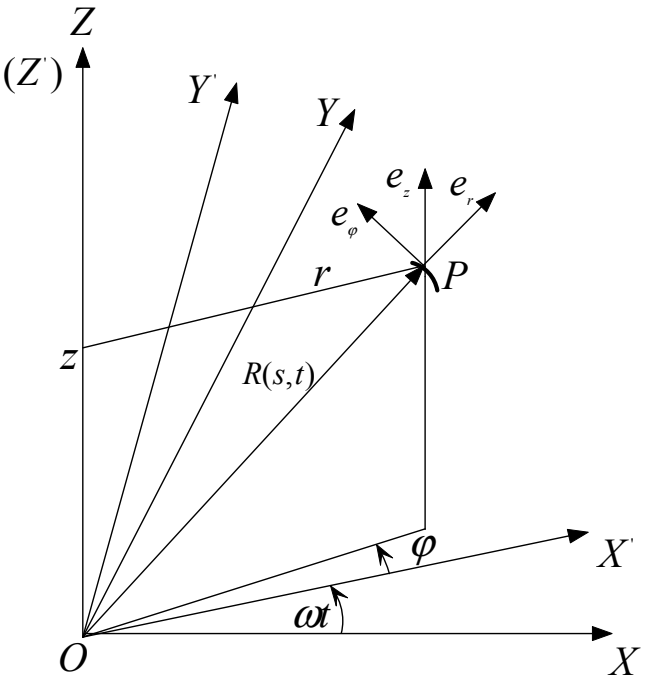

Figure 2: Inertial and rotating reference frames.

the yarn. The angular speed of the leaving point on the navel surface will vary as it moves along its trajectory (Figure 4).

The yarn is assumed to be flexible and uniform. It is reasonable to make the assumption that the yarn is inextensible, [Fraser, Ghosh and Batra, 1992] which results in

$$r_0^2\left(\frac{\partial\theta}{\partial s}\right)^2+[r_m+r_0(1-\cos\theta)]^2\left(\frac{\partial\varphi}{\partial s}\right)^2=1. \tag{3}$$

In the following analysis, we will consider three kinds of force acting on the yarn on the navel surface, namely internal tension force $T(s,\,t)$, friction force $\mathbf{F}\,(s,\,t)$ and normal reaction force $\mathbf{N}\,(s,\,t)$. The air drag and yarn weight are neglected since they have a smaller effect compared with the three kinds of forces mentioned above [Guo, Tao and Lo, 2000]. Thus, the time dependent equation for the motion of yarn element P is

$$m\left\{D^2R+2\omega e_z\times DR+\omega^2 e_z\times(e_z\times R)\right\}=\frac{\partial}{\partial s}\left(T\frac{\partial R}{\partial s}\right)+F+N, \tag{4}$$

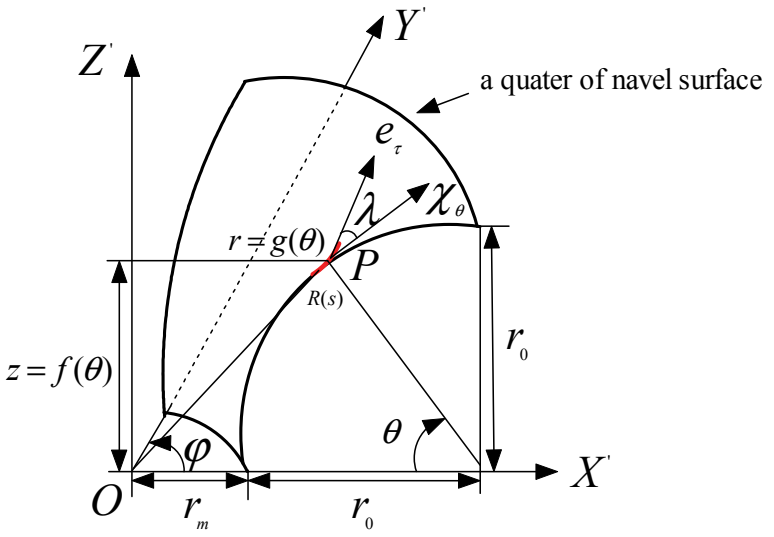

Figure 3: Navel coordinate systems and generatrix

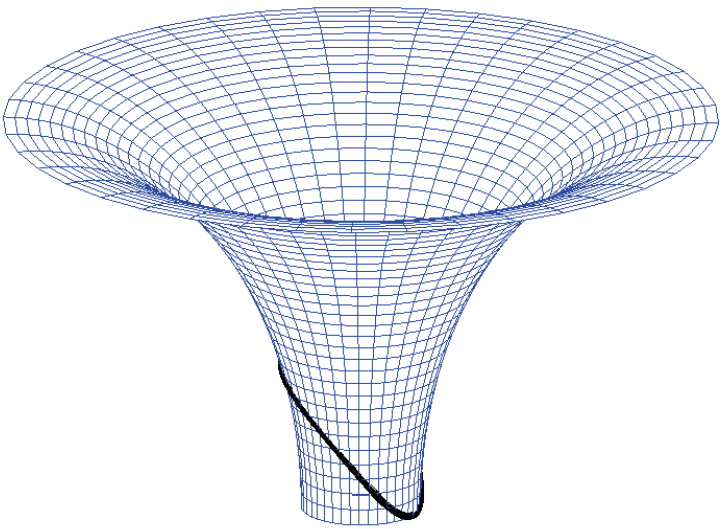

Figure 4: The navel surface and the trajectory of the leaving point of the yarn.

where m is the constant linear density of the yarn, and the operator $\mathbf{D}$ is given by

$$D = \frac{\partial}{\partial t} + \upsilon_0 \frac{\partial}{\partial s},$$

where υ_0 is the constant delivery speed of the yarn. The operator $\mathbf{D}$ is the total time derivative following the motion of P relative to the rotating frame. Thus $\mathbf{DR}$ is the velocity of the yarn element P and $\mathbf{D}^2\mathbf{R}$ is the acceleration relative to the rotating frame. The friction force acting on the yarn as it slides over the navel surface follows the Coulomb friction law:

$$F = -\mu \frac{v}{\|v\|}, \tag{5}$$

where $\mathbf{v} = \mathbf{DR} + \omega \mathbf{e}_z \times \mathbf{R}$. And the normal reaction force $\mathbf{N} = \|\mathbf{N}\|\mathbf{e}_n$, where $e_n = -\cos\theta\, e_r + \sin\theta\, e_z$, is the unit normal vector at the yarn element P on the navel. Accordingly, we have

$$N = \|N\|\, e_n = \|N\|\, (-\cos\theta\, e_r + \sin\theta\, e_z). \tag{6}$$

Since the motion of the yarn on the navel is apparently periodic, it is more convenient to impose periodic conditions on the solutions than initial conditions. Next, we formulate the periodic and boundary conditions for the problem to complete the model description. Let Γ be the period of the motion (i.e. the time for the leaving point of the yarn to complete one cycle around its trajectory on the navel). A periodic solution of the motion equation needs to satisfy the following conditions

$$\begin{cases} R(s,t+\Gamma) = R(s,t), \\ T(s,t+\Gamma) = T(s,t), \end{cases} \qquad 0 \le s \le s_l(t). \tag{7}$$

where $s_l(t)$ is the total length of yarn on the navel and it is time varying. It also satisfies the periodic condition that $s_l(t+\Gamma) = s_l(t)$. The first equation of (7) is equivalent to

$$\begin{cases} \theta(s,t+\Gamma) = \theta(s,t), \\ \varphi(s,t+\Gamma) = \varphi(s,t), \end{cases} \qquad 0 \le s \le s_l(t). \tag{8}$$

After leaving the navel surface, the yarn comes in contact with the fixed point A of the doffing tube, as shown in Figure 5. The coordinates of the point A are (r_m, 0, $-z_1$), $z_1 > 0$. The point Q_0 ($s = 0$) is the entrance point of yarn on the navel at $\theta = \pi/2$, while Q_1 ($s = s_l(t)$) is the leaving point of yarn element on the navel. After

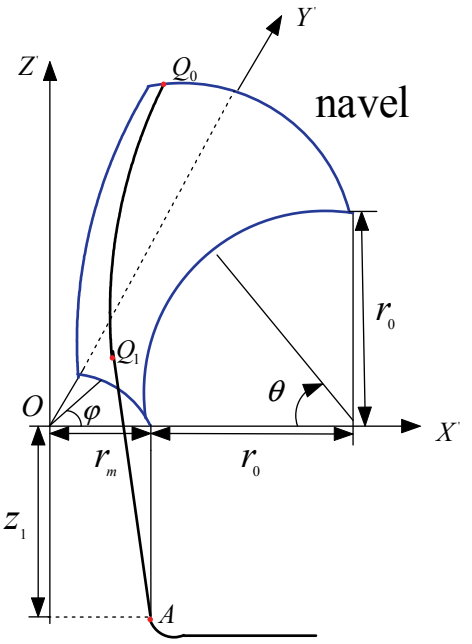

Figure 5: yarn trajectory between the entrance point Q_0 and the fixed point A

leaving the navel surface, the yarn finally moves out the navel through the doffing tube at the fixed point A, as shown in Figure 5.

Since Q_1A lies in the tangent plane of navel at the point Q_1, the parameters of the trajectory of Q_1 satisfies [Yu, Cai, Wu and Chen, 2007]

$$\tan\theta_l = \begin{cases} \frac{-z_1[r_0+r_m(1-\cos\varphi_l)]}{r_0^2-z_1^2} + \frac{r_0\sqrt{z_1^2+2r_0r_m(1-\cos\varphi_l)+r_m^2(1-\cos\varphi_l)^2}}{r_0^2-z_1^2}, & r_0 \neq z_1. \\ \frac{2r_m(1-\cos\varphi_l)r_0+r_m^2(1-\cos\varphi_l)^2}{2z_1[r_0+r_m(1-\cos\varphi_l)]}, & r_0 = z_1. \end{cases} \tag{9}$$

Thus, the curve of the trajectory of the leaving point is shown in Figure 4 (the bold black line).

Boundary conditions should be formulated at the entrance point Q_0 of the yarn on the edge of the navel

$$R(0,t) = (r_m + r_0)e_r + r_0 e_z, \quad i.e. \quad \theta(0,t) = \frac{\pi}{2}. \tag{10}$$

The radius vector form of the navel in the inertial frame is

$$\vec{\chi} = ([r_m + r_0(1-\cos\theta)]\cos\varphi,\ [r_m + r_0(1-\cos\theta)]\sin\varphi,\ r_0\sin\theta),$$

and the direction of the meridian line of the navel is defined by the unit vector of $\vec{\chi}_\theta$, where $\vec{\chi}_\theta$ is the partial derivative of $\vec{\chi}$ to θ. Define the deviate angle λ as the angle between the tangent vector of the yarn $\mathbf{e}_\tau$ and the meridian line of the navel at the yarn element P, as shown in Figure 3.

The parameters $\theta_l = \theta\ (s_l(t),\ t)$ and $\phi_l = \phi\ (\ s_l(t),\ t)$ of yarn position vector at the leaving point $s = s_l(t)$ must satisfy the trajectory Eq. (9). The corresponding position vector is $\mathbf{R}(s_l(t),t) = [r_m + r_0(1-\cos\theta_l)]\ \mathbf{e}_r + r_0\sin\theta_l\mathbf{e}_z$. Let λ_l be the angle between the tangent vector of the yarn and the meridian line at the leaving point, it is a periodic function of position vector of the leaving point on the navel. The tangent vector at this point is calculated as

$$\begin{aligned}\frac{\partial R(s_l,t)}{\partial s} &= \frac{R_\theta}{\|R_\theta\|}\cos\lambda_l + \sin\lambda_l e_\varphi = (\sin\theta_l e_r + \cos\theta_l e_z)\cos\lambda_l + \sin\lambda_l e_\varphi \\ &= \sin\theta_l\cos\lambda_l e_r + \sin\lambda_l e_\varphi + \cos\theta_l\cos\lambda_l e_z\end{aligned} \tag{11}$$

The velocity of the point relative to the rotating frame is

$$\begin{aligned}\frac{\partial R(s_l,t)}{\partial s} + \frac{\partial R(s_l,t)}{\partial s}(s_l,t)\frac{ds_l}{dt} = \\ r_0\sin\theta_l\frac{\partial\theta_l}{\partial t}e_r + [r_m + r_0(1-\cos\theta_l)]\frac{\partial\varphi_l}{\partial t}e_\varphi + r_0\cos\theta_l\frac{\partial\theta_l}{\partial t}e_z\end{aligned} \tag{12}$$

Notice that the absolute velocity vectors of any yarn element on the navel is $\frac{\partial R}{\partial t} + \upsilon_0\frac{\partial R}{\partial s} + \omega e_z \times R$. From the point of view of composition of velocities, this absolute velocity can be resolved into a constant velocity along $\overrightarrow{Q_1A}$ and a rotation speed $\frac{\partial\varphi}{\partial t}$ about Z axis, thus we can obtain the absolute velocity of the element at $s = s_l(t)$

$$\begin{aligned}\frac{\partial R}{\partial s}(s_l,t) + \upsilon_0\frac{\partial R}{\partial s}(s_l,t) + \omega[r_m + r_0(1-\cos\theta_l)]e_\varphi = \\ \upsilon_0\frac{\overrightarrow{Q_1A}}{\left\|\overrightarrow{Q_1A}\right\|} + [r_m + r_0(1-\cos\theta_l)]\frac{\partial\varphi_l}{\partial t}e_\varphi\end{aligned} \tag{13}$$

Notice that the right hand side of the above equation takes advantage of the continuity of tangent vector at the leaving point of the yarn. In the cylindrical coordinate

system,

$$\frac{\overrightarrow{Q_1A}}{\left\|\overrightarrow{Q_1A}\right\|} = \frac{\sqrt{[r_m + r_0(1-\cos\theta_l)]^2 + r_m^2 - 2r_m[r_m + r_0(1-\cos\theta_l)]\cos\varphi_l}}{\sqrt{[r_m + r_0(1-\cos\theta_l)]^2 + r_m^2 - 2r_m[r_m + r_0(1-\cos\theta_l)]\cos\varphi_l + (r_0\sin\theta_l + z_1)^2}} e_r + \frac{r_0\sin\theta_l + z_1}{\sqrt{[r_m + r_0(1-\cos\theta_l)]^2 + r_m^2 - 2r_m[r_m + r_0(1-\cos\theta_l)]\cos\varphi_l + (r_0\sin\theta_l + z_1)^2}} e_z \tag{14}$$

Subtracting Eq. (13) from Eq. (12), we then substitute Eq. (11) and Eq. (14) into the resultant equation and can obtain the formulas that govern the change rate of the yarn length of the yarn $s_l(t)$ between the entrance point of the yarn at the boundary of the navel where $\theta = \pi/2$ and the leaving point.

$$\left(\frac{ds_l}{dt} - \upsilon_0\right)\sin\lambda_l = \omega[r_m + r_0(1-\cos\theta_l)]. \tag{15}$$

The formulation of the problem and its corresponding periodic and boundary conditions are completed. These boundary conditions are critical for the construction of perturbation analysis that reduces the dependent problem to solving a series of stationary problems. The perturbation analysis will be carried out in the next section to obtain an approximate solution for the dynamic problem.

3 Perturbation Analysis

First, the dimensionless equation for the problem can be derived by appropriately scaling the governing Eq. (4) with length and time scales. We choose the period Γ of the leaving point around its trajectory on the navel as time scale and the height of the navel r_0 as length scale. In the following, a bar over a variable represents a dimensionless variable.

$$\begin{cases} \bar{R} = R/r_0 = (r_m/r_0 + 1 - \cos\theta)e_r + \sin\theta\, e_z, \\ \bar{s} = s/r_0, \quad \bar{t} = t/\Gamma, \quad \bar{v} = v/(\omega_0 a), \quad \bar{\upsilon}_0 = \upsilon_0/(\omega_0 a) \\ \bar{T} = T/(m\omega_0^2 a^2), \quad \bar{F} = F\, r_0/(m\omega_0^2 a^2), \quad \bar{N} = N\, r_0/(m\omega_0^2 a^2). \end{cases} \tag{16}$$

where ω_0 is the angular speed of the rotor, a is the radius of the rotor.

Accordingly, Eq. (4) can be formulated in terms of dimensionless variables as

$$\bar{D}^2\bar{R} + 2\Omega e_z \times \bar{D}\bar{R} + \Omega^2 e_z \times (e_z \times \bar{D}\bar{R}) = \frac{\partial}{\partial\bar{s}}\left(\bar{T}\frac{\partial}{\partial\bar{s}}R\right) + \bar{F} + \bar{N} \tag{17}$$

where

$$\bar{D} = \varepsilon \partial/\partial t + \bar{v}_0 \partial/\partial \bar{s}, \tag{18}$$

and

$$\varepsilon = \frac{r_0}{\omega_0 a \Gamma}, \quad \Omega = \frac{\omega r_0}{\omega_0 a}. \tag{19}$$

The dimensionless form of friction drag and the normal force are:

$$\bar{F} = -\mu \, \|\bar{N}\| \, \frac{\bar{v}}{\|\bar{v}\|}, \tag{20}$$

$$\bar{N} = \|\bar{N}\| \, (-\cos\theta \, e_r + \sin\theta \, e_z). \tag{21}$$

The periodic condition (7) and inextensible condition (3) become:

$$\begin{cases} \bar{R}(\bar{s}, \bar{t}+1) = \bar{R}(\bar{s}, \bar{t}), \\ \bar{T}(\bar{s}, \bar{t}+1) = \bar{T}(\bar{s}, \bar{t}), \end{cases} \qquad 0 \le \bar{s} \le \bar{s}_l(t) \tag{22}$$

and

$$\left(\frac{\partial \theta}{\partial \bar{s}}\right)^2 + \left(\frac{r_m}{r_0} + 1 - \cos\theta\right)^2 \left(\frac{\partial \varphi}{\partial \bar{s}}\right)^2 = 1. \tag{23}$$

The boundary condition at the entrance point and the leaving point become:

$$\bar{R}(0, \bar{t}) = (\frac{r_m}{r_0} + 1) e_r + e_z, \quad i.e. \quad \theta(0, \bar{t}) = \frac{\pi}{2} \tag{24}$$

and

$$\left(\varepsilon \frac{d\bar{s}_l}{d\bar{t}} - \bar{v}_0\right) \sin\lambda_l = \Omega \left(\frac{r_m}{r_0} + 1 - \cos\theta_l\right) \tag{25}$$

Notice that the mean angular speed ω and ω_0 have a slight difference, with ω ranging $0.85\omega_0 \sim 0.95\omega_0$, thus ε ranges $0.0524 \sim 0.05854$. This is small when compared with other parameters of the problem, such as tension of yarn, yarn position vector coordinates. Thus, it is feasible to make use of perturbation method to expend the position vectors, tension, and moving boundary quantities in powers of ε, and then obtain an approximation solution of the problem. In the following, expressions for

the desired solution in terms of a power series in "small" parameter ε are outlined. The position vector $\bar{R}(\bar{s},\bar{t})$ and tension $\bar{T}(\bar{s},\bar{t})$ are expended as follows:

$$\begin{cases} \bar{R}(\bar{s},\bar{t}) = \bar{R}_0(\bar{s},\bar{t}) + \varepsilon\bar{R}_1(\bar{s},\bar{t}) + \varepsilon^2\bar{R}_2(\bar{s},\bar{t}) + \cdots \\ \bar{T}(\bar{s},\bar{t}) = \bar{T}_0(\bar{s},\bar{t}) + \varepsilon\bar{T}_1(\bar{s},\bar{t}) + \varepsilon^2\bar{T}_2(\bar{s},\bar{t}) + \cdots . \end{cases} \tag{26}$$

The moving boundary needs to be imposed for this problem, thus the arc quantity $\bar{s}_l(\bar{t})$ must also be expended

$$\bar{s}_l(\bar{t}) = \bar{s}_{l0}(\bar{t}) + \varepsilon\bar{s}_{l1}(\bar{t}) + \varepsilon^2\bar{s}_{l2}(\bar{t}) + \cdots . \tag{27}$$

From Eq. (25), the parameter Ω depends on the deviate angle and it needs to be expended in powers of ε as well:

$$\Omega = \Omega_0 + \varepsilon\,\Omega_1 + \varepsilon^2\Omega_2 + \cdots . \tag{28}$$

The position vector parameters $\theta(\bar{s},\bar{t})$ and $\varphi(\bar{s},\bar{t})$ must also be expended similarly as follows

$$\begin{cases} \theta(\bar{s},\bar{t}) = \theta_0(\bar{s},\bar{t}) + \varepsilon\theta_1(\bar{s},\bar{t}) + \varepsilon^2\theta_2(\bar{s},\bar{t}) + \cdots \\ \varphi(\bar{s},\bar{t}) = \varphi_0(\bar{s},\bar{t}) + \varepsilon\varphi_1(\bar{s},\bar{t}) + \varepsilon^2\varphi_2(\bar{s},\bar{t}) + \cdots . \end{cases} \tag{29}$$

Under most settings in rotor spinning process, the deviate angle at the leaving point λ_l ranges between 0^o and 13^o, and the Taylor expansions of sin λ_l and cos λ_l are convergent. It is convenient to define $\lambda_l = \varepsilon\phi_l$, thus we have:

$$\begin{cases} \sin\lambda_l = \varepsilon\phi_l - \varepsilon^3\frac{1}{3!}\phi_l^3 + \cdots \\ \cos\lambda_l = 1 - \varepsilon^2\frac{1}{2}\phi_l^2 + \cdots . \end{cases} \tag{30}$$

Substituting Eq. (26) and Eq. (28) into Eq. (17), the zero order approximation equations of Eq. (17) can be given as

$$\bar{\upsilon}_0^2\frac{\partial^2\bar{R}_0}{\partial^2\bar{s}} + 2\bar{\upsilon}_0\Omega_0 e_z\times\frac{\partial\bar{R}_0}{\partial\bar{s}} + \Omega_0^2 e_z\times(e_z\times\frac{\partial\bar{R}_0}{\partial\bar{s}}) = \frac{\partial}{\partial\bar{s}}\left(\bar{T}_0\frac{\partial\bar{R}_0}{\partial\bar{s}}\right) + \bar{F}_0 + \bar{N}_0. \tag{31}$$

From the expansion (29), the zero order approximation for the inextensible condition yields:

$$\left(\frac{\partial\theta_0}{\partial\bar{s}}\right)^2 + \left(\frac{r_m}{r_0} + 1 - \cos\theta_0\right)^2\left(\frac{\partial\varphi_0}{\partial\bar{s}}\right)^2 = 1. \tag{32}$$

The terms $\bar{F}_0$ and $\bar{N}_0$ are accordingly given by:

$$\bar{F}_0 = -\mu \, \|\bar{N}_0\| \, \frac{\bar{v}_0}{\|\bar{v}_0\|}, \tag{33}$$

and

$$\bar{N}_0 = \|\bar{N}_0\| \, (-\cos\theta_0 e_r + \sin\theta_0 e_z). \tag{34}$$

respectively, where

$$\bar{v}_0 = \bar{\upsilon}_0 \frac{\partial R_0}{\partial \bar{s}} + \Omega_0 e_z \times R_0, \tag{35}$$

where the position vector $\bar{R}_0 = \left[\frac{r_m}{r_0} + 1 - \cos\theta_0\right] e_r + \sin\theta_0 e_z$.
The expansion form of Eq. (25) is

$$\begin{aligned} &\left(\varepsilon \frac{d\bar{s}_{l0}}{d\bar{t}} + \varepsilon^2 \frac{d\bar{s}_{l1}}{d\bar{t}} + \cdots - \bar{\upsilon}_0\right)\left(\varepsilon\phi_l - \varepsilon^3 \frac{1}{3!}\phi_l^3 + \cdots\right) \\ &= \Omega_0 \left(\frac{r_m}{r_0} + \frac{1}{2}\theta_0^2\right) + \varepsilon \left(2\Omega_0\theta_0\theta_1 + \Omega_1 \frac{r_m}{r_0} + \frac{\Omega_1}{2}\theta_0^2\right) + \cdots \end{aligned} \tag{36}$$

We can get from Eq. (36) that $\Omega_0 \left(\frac{r_m}{r_0} + \frac{1}{2}\theta_0^2\right) = 0$, which results in Ω_0=0. Eq. (31) is then reduced to

$$\bar{\upsilon}_0^2 \frac{\partial^2 \bar{R}_0}{\partial^2 \bar{s}} = \frac{\partial}{\partial \bar{s}} \left(\bar{T}_0 \frac{\partial \bar{R}_0}{\partial \bar{s}}\right) + \bar{F}_0 + \bar{N}_0 \tag{37}$$

Leaving out the subscript 0 in Eq. (37) for simplicity, its components form with the normal force and friction drag given by Eq. (34) and Eq. (33) together with the inextensibility condition lead to the following system

$$(\bar{\upsilon}_0^2 - \bar{T})(\cos\theta\theta'^2 + \sin\theta\theta'') = \bar{T}' \sin\theta\theta' - \mu \, \|\bar{N}\| \sin\theta\theta' - \|\bar{N}\| \cos\theta \tag{38}$$

$$(\bar{\upsilon}_0^2 - \bar{T}) \left[\sin\theta\theta'\varphi' + \left(\frac{r_m}{r_0} + 1 - \cos\theta\right)\varphi''\right] = \left(\bar{T}' - \mu \, \|\bar{N}\|\right) \left(\frac{r_m}{r_0} + 1 - \cos\theta\right)\varphi' \tag{39}$$

$$(\bar{\upsilon}_0^2 - \bar{T})(\cos\theta\theta'' - \sin\theta\theta'^2) = \bar{T}' \cos\theta\theta' - \mu \, \|\bar{N}\| \cos\theta\theta' + \|\bar{N}\| \sin\theta \tag{40}$$

$$\theta'^2 + \left(\frac{r_m}{r_0} + 1 - \cos\theta\right)^2 \varphi'^2 = 1 \tag{41}$$

where $'$ denotes $\frac{d}{d\bar{s}}$.

According to Eq. (11), the unit tangent vector at the leaving point can be given by

$$\begin{aligned}\frac{\partial \bar{R}}{\partial \bar{s}}(s_l) &= \sin\theta_l \frac{\partial \theta_l}{\partial \bar{s}} e_r + (\frac{r_m}{r_0} + 1 - \cos\theta_l)\frac{\partial \varphi_l}{\partial \bar{s}} e_\varphi + \cos\theta_l \frac{\partial \theta_l}{\partial \bar{s}} e_z \\ &= \sin\theta_l \cos\lambda_l e_r + \sin\lambda_l e_\varphi + \cos\theta_l \cos\lambda_l e_z.\end{aligned} \tag{42}$$

From the equation above, we have

$$\begin{cases}\theta'(s_l) = \cos\lambda_l \\ \varphi'(s_l) = \frac{\sin\lambda_l}{\frac{r_m}{r_0}+1-\cos\theta_l}\end{cases} \tag{43}$$

If Eq. (40) times $\sin\theta$ and Eq. (38) times $\cos\theta$ respectively, it will be observed from the substraction of the resultant two equations that

$$\|\bar{N}\| = (\bar{T} - \bar{v}_0^2)\theta'^2. \tag{44}$$

Taking the derivative of the constraint Eq. (41), we have

$$\theta''\theta' + \sin\theta\left(\frac{r_m}{r_0} + 1 - \cos\theta\right)\theta'\varphi'^2 + \left(\frac{r_m}{r_0} + 1 - \cos\theta\right)^2 \varphi''\varphi' = 0. \tag{45}$$

If Eq. (38) times $\sin\theta\theta'$, Eq. (40) times $\cos\theta\theta'$, and Eq. (39) times $(\frac{r_m}{r_0} + 1 - \cos\theta)\varphi'$, the resultant equations are added to give

$$\begin{aligned}\bar{T}' = (\bar{v}_0^2 - \bar{T})\left[\theta''\theta' + \sin\theta\left(\frac{r_m}{r_0} + 1 - \cos\theta\right)\theta'\varphi'^2 + \left(\frac{r_m}{r_0} + 1 - \cos\theta\right)^2 \varphi''\varphi'\right] \\ - \mu(\bar{v}_0^2 - \bar{T})\theta'^2\end{aligned} \tag{46}$$

Substituting Eq. (45) into Eq. (46), T' can be given by

$$\bar{T}' = \mu(\bar{T} - \bar{v}_0^2)\theta'^2. \tag{47}$$

For a given ϕ_l, we can compute the θ_l of the leaving point of the yarn by Eq. (9). Thus, the angle between the tangent vector of the yarn and the meridian line at the leaving point λ_l can be obtained from the equation below

$$\cos\lambda_l = \frac{[r_m + r_0(1-\cos\theta_l)]\sin\theta_l - r_m\sin\theta_l\cos\varphi_l + (r_0\sin\theta_l + z_1)\cos\theta_l}{\sqrt{[r_m + r_0(1-\cos\theta_l)]^2 + r_m^2 - 2r_m[r_m + r_0(1-\cos\theta_l)]\cos\varphi_l + (r_0\sin\theta_l + z_1)^2}} \tag{48}$$

The variation of deviate angle λ_l can be approximated by

$$\lambda_l(\varphi_l) = \lambda_{l\max} \sin\varphi_l + 0.0241 \sin(2\varphi_l). \tag{49}$$

It is easy to get the corresponding variation equation of deviate angle λ_l as a function of $\bar{t}$ with one period:

$$\lambda_l(\bar{t}) = \lambda_{l\max} \sin 2\pi\bar{t} + 0.0241 \sin 4\pi\bar{t}. \tag{50}$$

Notice that according to (48), λ_{lmax} changes as the geometry parameters of the navel r_m, r_0 and z_1 adjust.

If Eqs. (47) and (44) are substituted into Eq. (38), it will be found that

$$\sin\theta\,\theta'' = 0, \quad \forall\theta \in [0, \pi/2], \tag{51}$$

which results that θ¡å= 0. It means that θ ' = C, where C is a constant. Thus, we have

$$\theta'(0) = \theta'(s_l) = \theta'(\bar{s}) = \cos\lambda = \cos\lambda_l, \tag{52}$$

which leads to $\lambda = \lambda_l$ for any given time t. Similarly, we get

$$\varphi'(0) = \varphi'(s_l) = \frac{\sin\lambda_l}{\frac{r_m}{r_0} + 1 - \cos\theta_l}. \tag{53}$$

The tension of yarn at the entrance point can be obtained from that [Wang and Huang, 2000]

$$T(0) = m\upsilon_0^2 + \frac{m\omega_0^2\left(a^2 - R_e^2\right)\left(\frac{a}{2} - \frac{\upsilon_0}{\omega_0}\right) + \frac{1}{4}E\omega_0^2\left(a^4 - R_e^4\right)}{a - R_e\sin\lambda_e}, \tag{54}$$

where R_e is the radius of the entrance point of the yarn and is equal to r_m+r_0, and λ_e is the angle between the tangent vector of the yarn at the entrance point and the meridian line of the navel.

The components of motion equations are finally reduced to

$$\bar{T}' = \mu(\bar{\upsilon}_0^2 - \bar{T})\theta'^2 \tag{55}$$

$$\sin\theta\,\theta'\varphi' + \left(\frac{r_m}{r_0} + 1 - \cos\theta\right)\varphi'' = 0 \tag{56}$$

$$\theta'^2 + \left(\frac{r_m}{r_0} + 1 - \cos\theta\right)^2 \varphi'^2 = 1 \tag{57}$$

with $T(0)$ is given by Eq. (54), $\theta\ (0) = \frac{\pi}{2}$, $\theta'(0) = \theta'(\bar{s}_l) = \cos\lambda_l$, $\varphi'(0) = \varphi'(\bar{s}_l) = \frac{\sin\lambda_l}{\frac{r_m}{r_0}+1-\cos\theta_l}$, $\varphi(\bar{s}_l) = 2\pi\bar{t}$. And the normal force $\bar{N}$ can be calculated by Eq. (44). For a given time $\bar{t}_0$, we need only to solve this boundary value problem to approximate the yarn motion.

4 Numerical simulation

For different time t, we use shooting method to solve a two point boundary-value problems defined above. The numerical procedure is reduced to solve the initial-value problem of Eqs. (55), (56) and (57). For a prescribed $\phi(0)$ together with $\theta\ (0) = \frac{\pi}{2}$, $T(0)$ is given through dimensionless the yarn tension at s= 0 calculated by Eq. (54), and the derivatives information in Eqs. (52) and (53), the fourth order Runge-Kutta method is used to solve the initial value problem. $\phi(0)$ should be adjusted to satisfy the boundary condition $\varphi_l = \varphi_l(\bar{t})$ and the Secant rule is adopted to update the initial $\phi(0)$.

In Section 4.1, comparisons is made among yarn average tension, experimental data and theoretical results by others showing the superiority of our model. Yarn trajectories and the variations of yarn tension and yarn length on the navel are presented in Section 4.2. We also studies the effects of the design parameters of navel profile and position of the point A on the yarn motion and tension in this part.

4.1 Average tension compared with experimental and theoretical results by others

To illustrate the validity of the model, we firstly compare the numerical simulation results, the measurement data in [Lotka and Jackowski, 2003] and predicted values obtained from empirical formula T= $0.72m\omega_0^2a^2$ [Grosberg and Mansour, 1975] about the average yarn tension for different linear densities in Table 1. For convenience of comparison, we use the same working parameters of spinning machine as adopted in [Lotka and Jackowski, 2003]. The rotor rotational velocity is 45000 r.p.m., and the spinning velocity is 50 m/min. We can find that our modeling yarn tension values fit well the measurement data and are more accurate than the values calculated by empirical formula in [Grosberg and Mansour, 1975]. The rotation speed of rotor is another important influential factor on yarn tension. Similar comparison among our simulation results, the measurement data in [Grosberg and Mansour, 1975] and predicted values obtained from empirical formula is presented in Table 2 to reveal the effect of rotor speed on yarn tension. It is easy to see that our model performs better than empirical formula and accords with the measurement data. Thus, it can be concluded that the proposed model is an excellent approach to predict yarn tension in rotor spinning.

Table 1: Yarn tension for different linear densities.

Yarn linear density (g/km)	**Measured tension** (N)	**Predicted tension by [Grosberg and Mansour, 1975]** (N)	**Predicted tension by our model** (N)
25	0.3431	0.2914	0.3408
35	0.5000	0.4080	0.4772
45	0.6765	0.5245	0.6135
55	0.8137	0.6410	0.7498

Table 2: Yarn tension for different rotor rotation speed.

Rotor speed (r.p.m.)	**Measured tension** (N)	**Predicted tension by [Grosberg and Mansour, 1975]** (N)	**Predicted tension by our model** (N)
30,000	0.1176	0.1295	0.1088
40,000	0.1961	0.2302	0.1934
50,000	0.2745	0.3597	0.3022
60,000	0.4412	0.5180	0.4352
70,000	0.6078	0.7051	0.5924
80,000	0.8235	0.9210	0.7738
90,000	1.0196	1.1656	0.9793
100,000	1.2549	1.4390	1.2090

4.2 Periodical motion simulation

Firstly, we study the periodical motion of yarn, the variations of yarn length on the navel and the tension at the leaving point when the navel geometry factor and the location of point A are fixed. Afterwards, the effects of the location design of point A are examined. Finally, we try to figured out the influences of the navel profile design factor r_m/r_0 on yarn tension and yarn shape parameters along the yarn length.

Some numerical results are given as shown in Figure 6 - Figure 13. Table 3 lists the yarn and spinning parameters for simulations.

The parameters r_m=1.25$\times 10^{-3}m$, r_m/r_0=1/5, and ratio z_1/r_m=4 are used in calculations for Figure 6 - Figure 9. Figure 6 (a) gives the yarn configurations at different time steps in half a period of the motion on the navel, where a period is discreted into 20 time steps. To get a better view of the yarn paths on the navel, we put the

Table 3: Yarn and simulation parameters.

Quantity	**Units**(SI)	**Value**
Yarn linear density m	kg/m	1.83×10^{-5}
Angular speed of rotor ω_0	rad/s	3000π
Radius of rotor a	m	2×10^{-2}
Friction coefficient μ	-	0.37
Time step Δt	s	5×10^{-2}

navel upside down as shown in Figure 6 (b). Since the distance of the point Q_0 between two adjacent time steps along the navel border θ=π/2 increases when the time increases from 0 to 0.5, then we have that the angular velocity of the entrance point Q_0 becomes larger in the first half period. For clarity, we omit the next half a period yarn paths in this figure. In fact, the motion of yarn in a period is symmetry about time $\bar{t}$=0.5, and the angular velocity of the entrance point Q_0 decreases as the time $\bar{t}$ increases from 0.5 to 1. The variation of the total arc length of the yarn on the navel s_l and the tension at the leaving point of the yarn T_l through two complete periods of motion are shown

by Figure 7. As we can see, the length of the yarn on the navel will decrease in the first half a period, and then increase in the following half a period, which is consistent with the simulation results in Figure 6. Yarn tension curves along yarn length at different time steps in a period of motion are presented in Figure 8. The tension of the leaving point not only depends on the length of the yarn on the navel but also depends on the tension at the entrance point which is dominated by the deviate angle λ_e, that is why the variations curves for s_l and T_l have much difference. Figure 9 shows the variations of θ and ϕ between the entrance point $\bar{s}$=0 and the leaving point $\bar{s} = \bar{s}_l$ through two periods of motion. Larger $\Delta\theta$ reflects that the leaving point of yarn is much closer to the lower edge of the navel (θ = 0). And larger $|\Delta\phi|$ shows that the yarn shape deviates further from the longitude of the navel. Thus, we can see from Figure 9 that the distance between the leaving point and the lower edge of the navel increases firstly and then decreases in a period of yarn motion, which is consistent with the trajectory of the leaving point on the navel. The deviation between the yarn path and the longitude of the navel reflected by Figure 9 is also in accord with the yarn shapes in Figure 6.

The effects of ratio z_1/r_m on the yarn tension and yarn shape parameters at a quarter of a cycle time (at the sixth time step) are shown in Figure 10 and Figure 11, respectively. As shown in Figure 10, larger z_1/r_m ratio decreases tension of yarn and increase the yarn length on the navel, and the resultant tension of the leaving point increases as the ratio increases. From Figure 11, it can be observed that

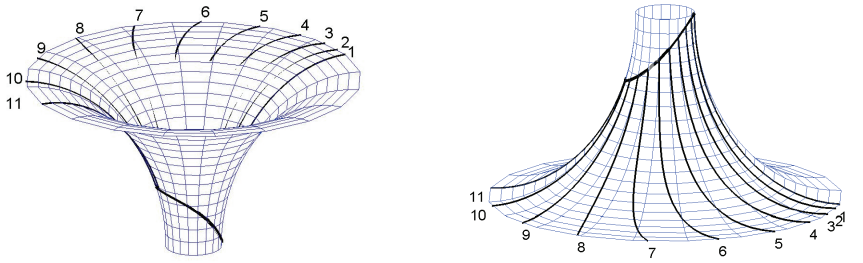

(a) Yarn shapes on the navel.

(b) Yarn shapes on the upturned navel.

Figure 6: yarn shapes at different time steps in half a period, the numbers i denotes the yarn shape at the i-th time step.

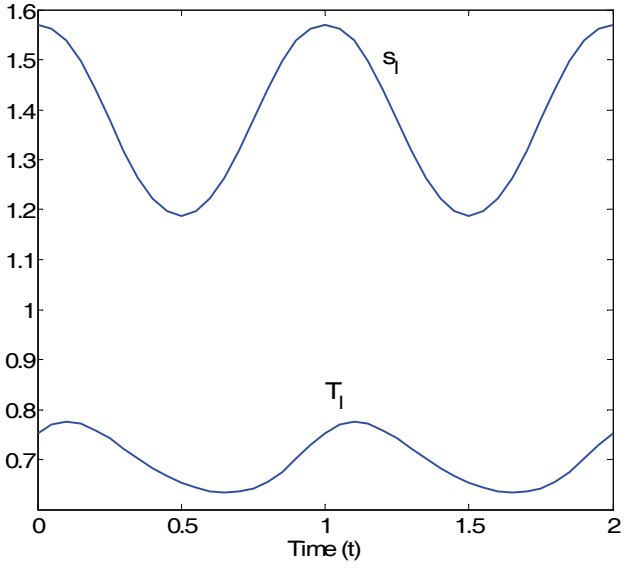

Figure 7: Variation of the total length of yarn s_l and yarn tension at the leaving point T_l through two periods of yarn motion on the navel.

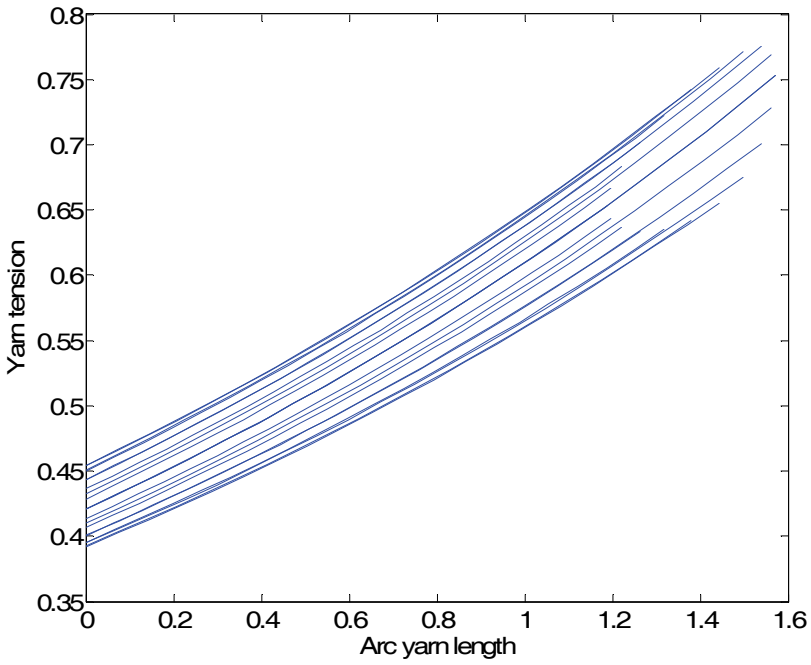

Figure 8: Tension along yarn length at different time steps during a period of motion on the navel.

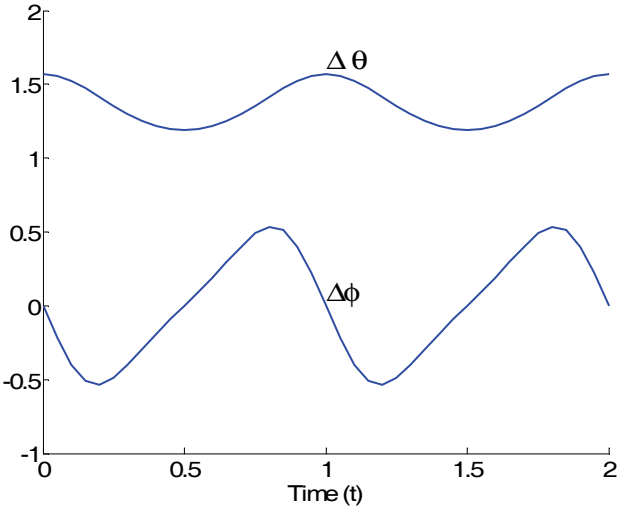

Figure 9: The difference of θ and ϕ between the entrance points and the leaving points at different time steps during two periods of motion on the navel.

larger z_1/r_m ration decreases the variation of ϕ and increases that of θ between the entrance point and the leaving point at a certain time.

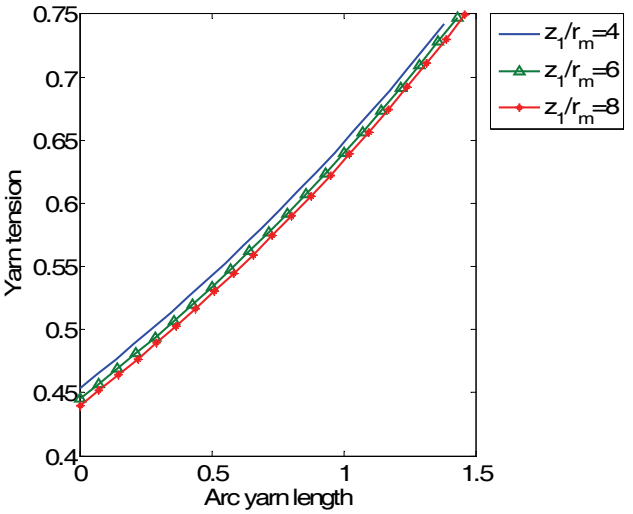

Figure 10: Tension of yarn at a quarter of a cycle time (at the sixth time step) for the ratios z_1/r_m= 4, z_1/r_m= 6, z_1/r_m= 8.

The effects of the design parameter r_m/r_0 of the navel profile are shown in Figure 12 and Figure 13. In Figure 12, it can be observed that as ratio r_m/r_0 grows, the tension in yarn becomes larger. The following Figure 13 shows that larger ratio r_m/r_0 can also cause smaller variations of ϕ between the entrance point and the leaving point. The variation of θ does not change markedly.

5 Conclusion

In this paper, we have proposed a nonlinear dynamic model for periodic analysis of slender threadline structures by perturbation analysis. The formulation of a perturbation expansion has been used to solve the time dependent problem with a sequence of quasi-steady state solutions. The moving boundary conditions are derived and the zero order approximation solution of the problem is determined by the moving boundary conditions. As an application of this proposed modeling method, dynamics of slender yarns produced in rotor spinning has been analyzed. The average tension simulations are more reliable than the results obtained by earlier work and show good agreements with measurement data. The model can show the motions of the yarn through a period of motion along its trajectory. The obtained nu-

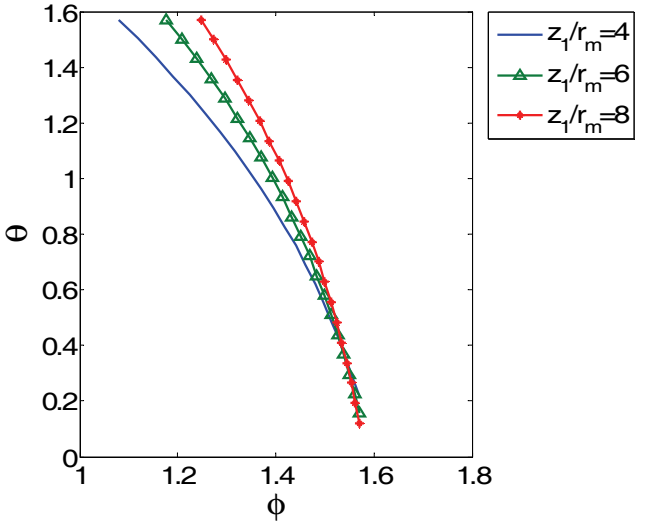

Figure 11: θ and ϕ relation at a quarter of a cycle time (at the sixth time step) for the ratios z_1/r_m= 4, z_1/r_m= 6, z_1/r_m= 8.

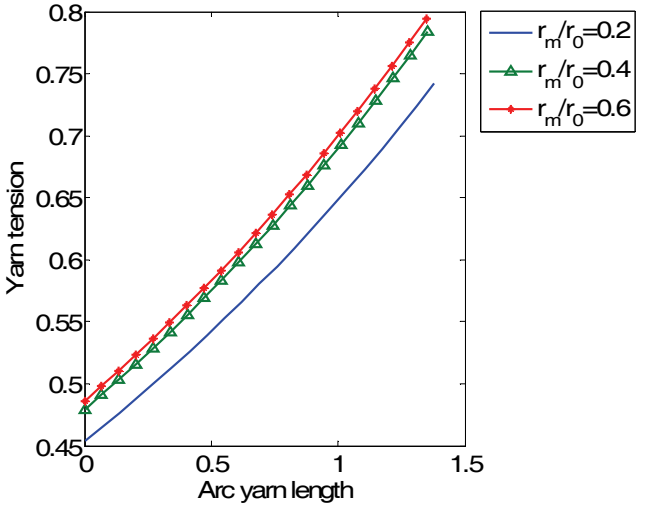

Figure 12: Tension of yarn at a quarter of a cycle time (at the sixth time step) for ratios r_m/r_0= 0.2, r_m/r_0= 0.4,r_m/r_0= 0.6.

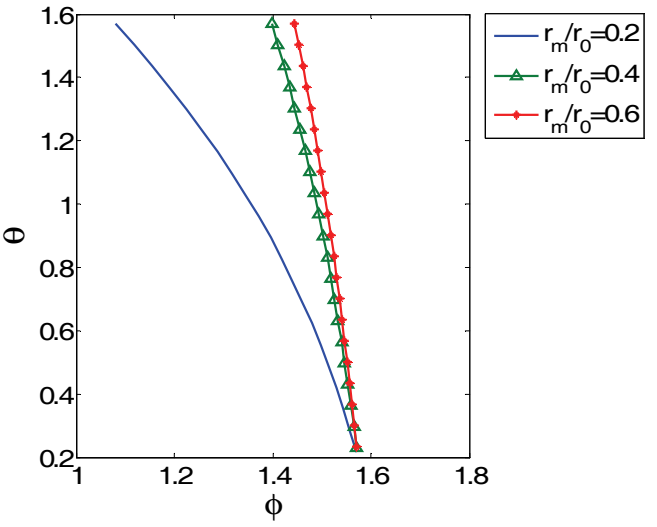

Figure 13: θ and ϕ relation at a quarter of a cycle time (at the sixth time step) for ratios r_m/r_0= 0.2, r_m/r_0= 0.4, r_m/r_0= 0.6.

merical results demonstrate that the arc length on the navel and the tension change with time periodically as it is moving on the navel. We also numerically consider the effects of navel geometry factors on the yarn tension and geometrical shapes. Moreover, the model is believed to be applicable to more complicated geometries. The proposed modeling and perturbation approximation procedure is a potential and practical way to deal with periodical problems of a group of slender thread like bodies.

Acknowledgement: The authors wish to acknowledge the funding support from the Hong Kong Polytechnic University for the work reported here.

References

Ayse Okur, S. K. (2006): Relationships Between Yarn Diameter/Diameter Variation and Strength. *Fibres & Textiles in Eastern Europe*, vol. 14, pp. 84-87.

Clark, J. D.; Fraser, W. B.; Stump, D. M. (2001): Modelling of Tension in Yarn Package Unwinding. *Journal of Engineering Mathematics*, vol. 40, no. 1, pp. 59-75.

Coleman, B. D.; Olson, W. K.; Swigon, D. (2003): Theory of Sequence-dependent DNA Elasticity. *Journal of Chemical Physics*, vol. 118, no.15, pp. 7127-7140.

Coyne, J. (1990): Analysis of the formation and elimination of loops in twisted cable, *IEEE J. Oceanic Eng.*, vol. 15, no. 2, pp. 72-83.

Fraser, W. B.; Ghosh, T. K.; Batra, S. K. (1992): On Unwinding Yarn from a Cylindrical Package. *Proceedings of the Royal Society A*, pp. 479-497.

Fraser, W. B.; Stump, D. M. (1998): Yarn Twist in the Ring-spinning Balloon. *Proceedings of the Royal Society A*, pp. 707-723.

Grosberg, P.; Mansour, S. A. (1975): Yarn Tension in Rotor-spinning. *Journal of the Textile Institute*, vol. 66, no. 6, pp. 228-231.

Grosberg, P.; Monsour, S. A. (1975): High-speed Open-end Rotor Spinning. *Journal of the texitile institute*, vol. 66, no. 11, pp. 389-396.

Guo, H. F.; Xu, B. G. (2010) A 3D Numerical Model for a Flexible Fiber Motion in Compressible Swirling Airflow, *CMES-Computer Modeling in Engineering & Sciences*, vol. 61, no. 3, pp. 201-222

Guo, H. F.; Xu, B. G. (2009): A Novel Method for Dynamic Simulation of Flexible Fibers in a 3D Swirling Flow. *International Journal of Nonlinear Sciences and Numerical Simulation*, vol. 10, no. 11-12, pp. 1473-1479.

Guo, P.; Tao, X. M.; Lo, T. (2000): A Mechnical Model of Yarn Twist Blockage in Rotor Spinning. *Textile Research Journal*, vol. 70, no. 1, pp. 11-17.

Heijden, G. H. M.; Neukirch, S.; Goss, V. G. A.; Thompson, J. M. T. (2003): Instability and self-contact phenomena in the writhing of clamped rods, *Int. J. Mech. Sci.*, vol. 45, no. 1, pp. 161-196.

Jurak, M.; Tambca, J. (1999): Derivation and Justification of a Curved Rod Model. *Mathematical Models and Methods in Applied Sciences*, vol. 9, no. 7, pp. 991-1014.

Kinkaid, N. M.; O'Reilly, O. M. (2001): On the Steady Motions of a Rotating Elastic Rod. *Journal of Applied Mechanics*, vol. 68, no. 5, pp. 766-771.

Kmoch, P.; Bonanni, U.; Magnenat-Thalmann, N. (2009): *Hair Simulation Model for Real-time Environments*. Computer Graphics International, Victoria, British Columbia, Canada, pp. 5-12.

Lotka, M.; Jackowski, T. (2003): Yarn Tension in the Process of Rotor Spinning. *AUTEX Research Journal*, vol. 3, pp. 1-5.

Lu , C. L.; Perkins, N. C. (1994): Nonlinear spatial equilibria and stability of cables under uniaxial torque", *J. Appl. Mech. T. ASME*, vol. 61, no. 4, pp. 879-886.

Lu, C. L.; Perkins N. C. (1995): Complex spatial equilibria of U-joint supported cables under torque, thrust and self-weight, *Int. J. non-Linear Mech.*, vol. 30, no.

3, pp. 271-285

Luo, A. C. J. (2000): A Nonlinear Theory for Traveling and Spinning, Sagged, Elastic Cables. *International Journal of Nonlinear Sciences and Numerical Simulation*, vol. 1, pp. 207.

Narayana, V. P. S. (2005): Novel Method for Dynamic Yarn Tension Measurement and Control in Direct Cabling Process. *Ph.D. thesis*, `http://gradworks.umi.com/32/23/3223208.html`.

O'Reilly, O. M. (1996): Steady Motions of a Drawn Cable. *Journal of Applied Mechanics*, vol. 63, no.1, pp. 180-189.

Tang, H.B.; Xu, B.G.; Tao, X.M. (2010): A New Analytical Solution of the Twist Wave Propagation Equation with Its Application in a Modified Ring Spinning System. *Textile Research Journal*, vol. 80, no. 7, pp.636-641.

Tang, H. B.; Xu, B. G.; Tao, X. M.; Feng, J. (2011): Mathematical Modeling and Numerical Simulation of Yarn Behavior in a Modified Ring Spinning System. *Applied Mathematical Modelling*, vol. 35, no. 1, pp. 139-151.

Tang, W. Z.; Advani S. G. (2005): Dynamic Simulation of Long Flexible Fibers in Shear Flow, *CMES-Computer Modeling in Engineering & Sciences*, vol. 8, no. 2, pp. 165-176

Tobias, I.; Swigon D.; Coleman, B. D. (2000): Elastic stability of DNA configurations. I. General theory, *Phys. Rev. E*, vol. 61, no. 1, pp. 747-758.

Wang, J.; Huang, X. B. (2000): Yarn Tension at Peeling Off Point in Rotor Spinning. *Journal of China Textile University English Edition*, vol. 17, pp. 14-17.

Xu, B. G.; Tao, X. M. (2003): Integrated Approach to Dynamic Analysis of Yarn Twist Distribution in Rotor Spinning: Part I: Steady State. *Textile Research Journal*, vol. 73, no. 1, pp. 79-89.

Yang, R. H.; Wu, Y.; Wang, S. Y. (2009): Tension of Rotor-spun Composite Yarn during Spinning Process. *International Journal of Nonlinear Sciences and Numerical Simulation*, vol. 10, pp. 903-906.

Yang, T. Z.; Fang, B.; Chen, Y.; Zhen, Y. X. (2009): Approximate Solutions of Axially Moving Viscoelastic Beams subject to Multi-frequency Excitations. *International Journal of Non-Linear Mechanics*, vol. 44, no. 2, pp. 230-238.

Yu, Z. H.; Cai, X. C.; Wu, W. Y.; Chen, R. Q. (2007): The yarn curve and tension in rotor spinning. *Jounal of Donghua University English Edition*, vol. 24, pp. 165-172.